RSC Advances

PAPER

View Article Online
View Journal | View Issue

Cite this: *RSC Adv.*, 2025, **15**, 15276

Properties and applications of two melt-cast cocrystal carriers†

Yunshu Zhao, [a] Yibo Zhou,[a] Jianping Song,[b] Fei Wang,[a] Xu Zhou,[b] Xiaoyan Zhang,[a] Shanhu Sun, *[a] Li Su,[a] Zhirong Suo,[a] Jinjiang Xu[b] and Jie Sun *[b]

To further investigate the feasibility of cocrystal explosives as melt-cast carriers, two types of energetic cocrystals were studied: 2,4-dinitroanisole (DNAN)/2-nitroaniline (NA) and ammonium dinitramide (ADN)/urea. The synthesis of these cocrystal materials was confirmed by comparing their X-ray diffraction (XRD) patterns with single-crystal simulation curves. Thermal stability was assessed using differential scanning calorimetry (DSC). *In situ* XRD was used to analyze the changes in the crystal structure of the two cocrystal carriers across varying temperatures. Additionally, the solubility and polymorphic transformation of ε-hexanitrohexaazaisowurtzitane (ε-CL-20) within these cocrystal carriers were analyzed using high performance liquid chromatography (HPLC) and XRD. The results reveal that the two cocrystal carriers exhibit satisfactory thermal stability. Their melting points are 69.3 °C and 71.9 °C and their decomposition temperatures are 319.8 °C and 201.9 °C, respectively. Additionally, they remain in their cocrystal phases after undergoing melting–solidification thermal cycles within the temperature range of 30–70 °C. The solubility of CL-20 in the DNAN/NA and ADN/urea cocrystal carriers is 3.274 g and 1.046 g, respectively, both significantly lower than that in DNAN. Additionally, it was observed that the polymorphic transformation of ε-CL-20 did not occur during the melting and casting process. Therefore, the DNAN/NA and ADN/urea cocrystals hold promise as novel melt-cast explosive carriers.

Received 8th April 2025
Accepted 28th April 2025

DOI: 10.1039/d5ra02417j

rsc.li/rsc-advances

1 Introduction

The ammunition charge is a critical element in ammunition production, serving as the foundation for achieving effective destructive performance of weapons and ensuring safety and reliability throughout the usage process.[1–3] Existing charging technologies can be categorized into three primary types: casting charge, pressure charge, and plastic charge. Among them, the casting charge is notable for its low production cost, high filling efficiency, and strong structural adaptability, making it one of the most important methods for warhead charging.[4–7] The performance of melt-cast explosives is influenced by various factors, with the melt-cast carrier playing a crucial role in determining their overall performance. As is known, an ideal melt-cast explosive carrier typically has the following characteristics: (1) high energy with excellent safety performance; (2) appropriate melting point; (3) sufficiently large temperature gap between the melting point and the decomposition temperature; (4) low vapor pressure and minimal inhalation toxicity; (5) good compatibility with other components.[8–10] Traditional melt-cast explosive carriers, such as TNT, suffer from several drawbacks, including low energy, poor mechanical properties, oil leakage, and high toxicity during production and use. These limitations hinder their ability to satisfy the evolving demands of modern weaponry and equipment development.[11–14] Therefore, there is a pressing need for a new melt-cast explosive carrier to replace TNT and improve the overall performance of weapons and ammunition.

In recent years, numerous new high energy-density melt-cast carrier explosives have been reported, both domestically and internationally, including 1,3,3-trinitroazetidine (TNAZ),[15,16] bis(4-nitrofurazan-3-yl)furazan (DNTF),[17,18] and 1-methyl-3,4,5-trinitropyrazole (MTNP).[19] However, the melting points of TNAZ (101 °C) and DNTF (110 °C) exceed the upper limit for steam melting, making them difficult to process using the traditional steam pouring process. Consequently, they cannot be used on their own as a melt-cast explosive carrier. To overcome this challenge, researchers have uniformly mixed two or more energetic compounds in precise ratios to form eutectic mixtures with a melting point lower than that of any component.[20–23] For instance, Wang *et al.*[24] prepared a DNAN/3,5-difluoro-2,4,6-trinitroanisole (DFTNAN) eutectic mixture in 2021, and reported that the volume shrinkage of DNAN/DFTNAN decreased by 6.5% while the melting point

[a]*School of Materials and Chemistry, Southwest University of Science and Technology, Mianyang 621010, Sichuan, People's Republic of China. E-mail: shanhusun@126.com*
[b]*Institute of Chemical Materials, China Academy of Engineering Physics, Mianyang 621900, Sichuan, People's Republic of China. E-mail: sunjie@caep.cn*

† Electronic supplementary information (ESI) available. See DOI: https://doi.org/10.1039/d5ra02417j

decreased by 36.6 °C compared with DNAN. Similarly, Zhu *et al.*[25] prepared a 1-methyl-2,4-dinitroimidazole (2,4-MDNI)/DNTF binary deep eutectic mixture in 2022, which did not only have an appropriate melting point (92.7 °C) but also reduced the sensitivity of DNTF while maintaining high energy performance. In the same year, Song *et al.*[26] successfully prepared the lowest eutectic mixture with MTNP and TNAZ, achieving significantly lower melting points and mechanical sensitivities compared with the individual components. However, the eutectic carrier is a multi-component aggregate with complex phase interfaces.[27] After undergoing a complex solid–liquid–solid transition during the melt-casting process, the probability of defects such as cracks and shrinkage cavities between the components is significantly higher compared with using a single carrier, which affects the charge quality of the ammunition. Consequently, modifying melt-cast carriers remains a significant technical challenge.

Recent studies have demonstrated that cocrystal technology, which combines two or more compounds through intermolecular non-covalent bonds to form crystals with specific structures and properties, can effectively reduce the melting points of explosives.[28–31] In 2019, the authors' group[32] prepared a DNAN/NA cocrystal with a melting point of 67.5 °C, which is 27.5 °C lower compared with that of DNAN (95 °C). This cocrystal demonstrated superior overall performance compared with the traditional melt-cast carrier, TNT. In 2022, Yang *et al.*[33,34] reported a 1,3,5-trinitrobenzene (TNB)/1,4-dinitroimidazole (1,4-DNI) cocrystal with a melting point of 84.4 °C, which is significantly lower than that of TNB (123.5 °C) and 1,4-DNI (91 °C). This cocrystal achieves superior detonation performance compared with TNT. In the same year, Bellas *et al.*[35] reported an ADN/urea cocrystal, envisioned as a novel melt-cast explosive carrier, with a melting point of 69.2 °C. However, research on cocrystal explosives used as melt-cast carriers is still at the stage of basic experimental exploration. Therefore, systematically investigating the comprehensive properties of existing melt-cast cocrystal carriers and evaluating their application potential is of great significance.

In this study, the comprehensive properties of DNAN/NA and ADN/urea cocrystals were investigated using DSC, *in situ* XRD, and scanning electron microscopy (SEM). Furthermore, the solubility and polymorphic transformation of the high-energy explosive CL-20 in the two cocrystal carriers were investigated, and the feasibility of using this cocrystal as a melt-cast carrier was preliminarily evaluated. The finding of this study provide a theoretical reference for the design, optimization, and application of energetic cocrystals as melt-cast carriers.

2 Experimental section

2.1 Materials

2,4-Dinitroanisole (DNAN) and ammonium dinitramide (ADN) were self-made in the laboratory. 2-Nitroaniline (NA) was purchased from Chengdu Gracia Chemical Technology Co., Ltd; urea purchased from Cologne Chemicals Co., Ltd; acetone and acetonitrile are commercially available analytically pure.

2.2 Preparation of cocrystal carrier

2,4-Dinitroanisole(198 mg, 1 mmol) and 2-nitroaniline (138 mg, 1 mmol) were added to 20 mL acetone solution to form a saturated solution. At room temperature, with the solvent slowly volatilizing, DNAN/NA cocrystals were precipitated from the solution after about 2 days.

Urea (194 mg, 3.2 mmol) and ammonium dinitramide (200 mg, 1.6 mmol) were added to 15 mL anhydrous acetonitrile to form a saturated solution. Then it was placed in a dryer equipped with a color-changing silica gel, and the solvent was slowly volatilized at room temperature. About a week later, the ADN/urea cocrystal was precipitated from the solution.

2.3 Solubility test of CL-20 in melt-cast carriers

Preparation of standard solutions, 50 mg, 20 mg, 5 mg, 4 mg, 0.8 mg CL-20 and 50 mg, 20 mg, 10 mg, 2 mg, 1 mg DNAN, DNAN/NA, and ADN/urea were accurately weighed. In a 50 mL volumetric flask, a series of standard solutions were prepared with acetonitrile (Fig. S5–7†).

Preparation of samples for solubility tests, the DNAN, DNAN/NA, and ADN/urea carriers (1.5 g) were added into different glass test tubes, heated to 100 °C in an oil bath, and kept warm for 5 min to ensure that the three carrier samples were completely melted. Then 0.2 g CL-20 was added and stirred continuously, and the samples were mixed well and then kept at 100 °C for 30 min. The supernatant of each group of samples was aspirated three times for chromatographic analysis (Table S4†).

2.4 Polymorphic transformation test of ε-CL-20 in melt-cast carriers

The DNAN/NA and ADN/urea carriers (0.5 g) were put into two glass test tubes. The oil bath was heated to 100 °C for 5 min to ensure that the explosives of the two carriers melted completely. Then 0.5 g ε-CL-20 samples were added and stirred continuously. After the samples were evenly mixed, they were kept for 30 min. Subsequently, the supernatant was poured out, and the remaining part was poured into an anti-static plastic bag to be ground into powder and washed three times with anhydrous ethanol. The washed CL-20 sample was placed on a filter paper and dried naturally for qualitative analysis of the crystal form.

2.5 Characterization

The thermal decomposition properties of the samples were tested by SDT Q600 synchronous thermal analyzer. The test temperature was 50–450 °C, the heating rate was 10 °C min^{-1}, the N_2 atmosphere, the N_2 flow rate was 50 mL min^{-1}, and the sample mass was less than 2.0 mg.

The XRD data were collected by Bruker D8 Advanced X-ray diffractometer at 40 kV and 40 mA with Cu Kα radiation (λ = 1.54180 Å). The detector is a Vant detector with a scanning range of 5–50°(2θ), and a scanning rate of $2°\cdot s^{-1}$. The *in situ* temperature control program was heated from 30 °C to 75 °C at a rate of 0.1 °C s^{-1}, and the first scan was started at 30 °C. Subsequently, the sample was scanned every 5 °C for 2 min

before each scan, and then the temperature was reduced from 75 °C to 30 °C at the same temperature control rate, and the 30 °C sample was scanned again.

The morphology of the samples were measured on Ultra55 field emission scanning electron microscope produced by Carl Zeiss, Germany. The protective gas was N_2, the current was set to 20 mA, the operating voltage was set to 7 kV, and the magnification was 100× to 1000×.

The solubility of the sample was determined by HPLC (UltiMate 3000 DGLC). The chromatographic analysis conditions were as follows: Zorbax SB C18 column (250 mm × 4.6 mm, 5.0 μm); mobile phase: acetonitrile/water (70 : 30); flow rate: 1.0 mL min^{-1}; detection wavelength: 254 nm; column temperature: 30 °C; injection volume: 5 μL.

3 Results and discussion

3.1 Thermal stability

Single-crystal XRD data (Table S1†) of the two energetic cocrystals were obtained by single-crystal X-ray diffraction (SXRD). The results matched literature-reported single-crystal data, confirming the successful synthesis of both cocrystals. The intermolecular interactions of DNAN/NA (Fig. S1 and Table S2†) and ADN/urea (Fig. S2 and Table S3†) cocrystals were analyzed. Results revealed that hydrogen bonding acts as the primary driving force for their formation. The purity of DNAN/NA and ADN/urea cocrystals was analyzed by powder X-ray diffraction, as shown in Fig. 1. The powder XRD diffraction patterns of DNAN/NA and ADN/urea are consistent with the cocrystal powder XRD diffraction patterns obtained by single crystal structure simulation, and the characteristic diffraction peak positions are the same basically, indicating that the prepared DNAN/NA and ADN/urea cocrystals have high purity.

The thermal stability of DNAN/NA and ADN/urea was evaluated by DSC. As shown in Fig. 2, the DSC curve of DNAN/NA cocrystal explosive shows that the endothermic peak begins to appear at 67.1 °C, with a peak temperature of 69.25 °C. Combined with the decrease in *in situ* XRD crystallinity and the disappearance of diffraction peaks near 65 °C (Fig. 3a), confirming that the process is an endothermic phenomenon caused by cocrystal melting. The exothermic peak begans at 296.42 °C, with a peak temperature of 319.76 °C, indicating that the cocrystal undergoes chemical decomposition.

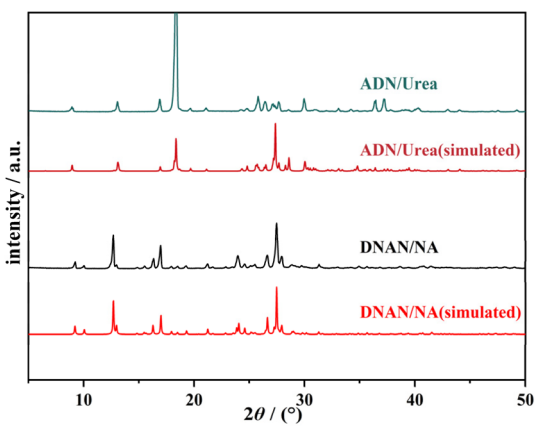

Fig. 1 The powder XRD patterns of DNAN/NA and ADN/urea cocrystals.

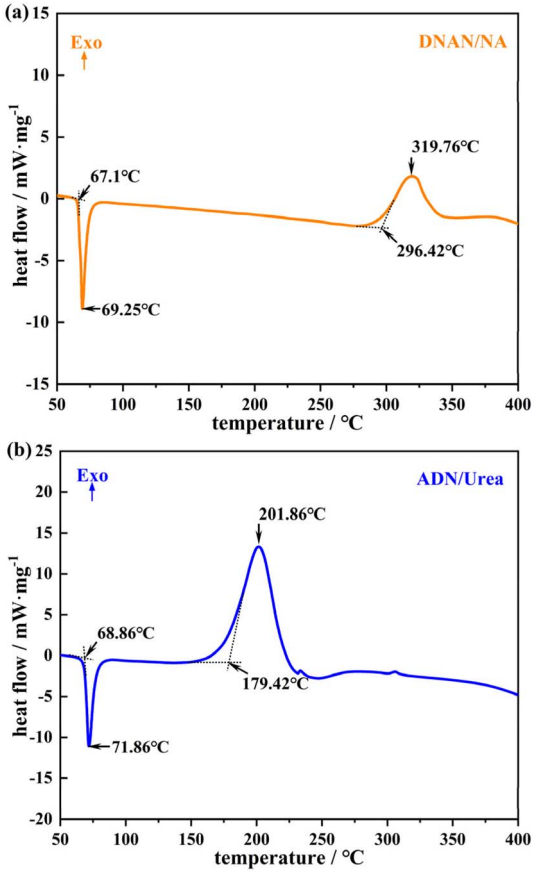

Fig. 2 (a) DSC curves of the DNAN/NA cocrystal, (b) DSC curves of the ADN/urea cocrystal.

For the ADN/urea cocrystal explosive, the DSC curve shows an endothermic peak at 68.86 °C, with a peak temperature of 71.86 °C, confirming the presence of an endothermic melting phenomenon within this temperature range. The exothermic peak begins at 179.42 °C, with a peak temperature of 201.86 °C, corresponding to the thermal decomposition process of the cocrystal. These results demonstrate that both DNAN/NA and ADN/urea cocrystal explosives exhibit suitable melting point and decomposition temperature, which are in line with the thermal performance index of the melt-cast explosive carrier.

3.2 *In situ* X-ray diffraction

The crystal structure changes of DNAN/NA and ADN/urea at varying temperatures were analyzed by *in situ* XRD. As shown in Fig. 3a and S3a,† the DNAN/NA cocrystal does not produce new characteristic diffraction peaks when heated to 65 °C. However, the diffraction peaks gradually shift toward lower angles as the temperature increases. For example, the diffraction peak of the (2 0–2) crystal plane shifted from $2\theta = 27.404°$ to 27.187°, indicating that the DNAN/NA cocrystal only undergoes thermal

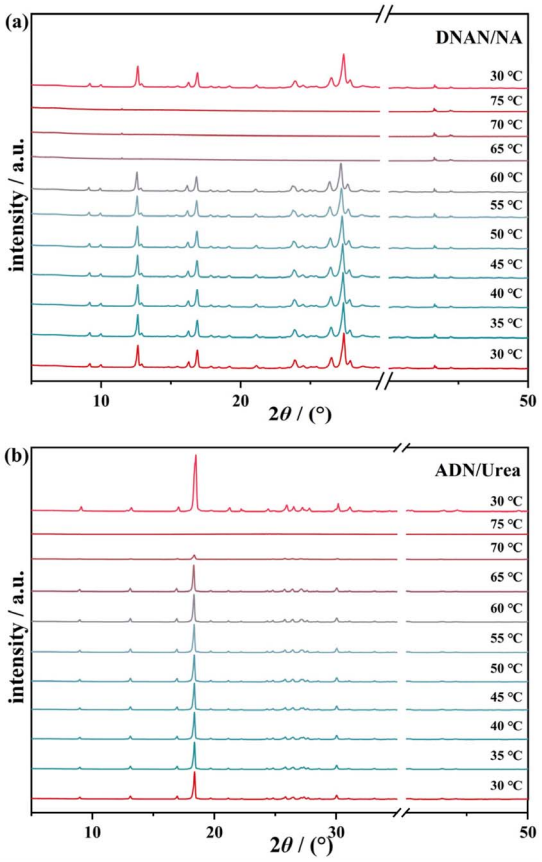

Fig. 3 (a) *In situ* XRD patterns of DNAN/NA cocrystal, (b) *in situ* XRD patterns of ADN/urea cocrystal.

expansion of its crystal structure with in this temperature range without undergoing any polymorphic transformation. When the heating temperature exceeds 65 °C, the diffraction peaks of the cocrystal gradually disappear, indicating that the cocrystal melted at this temperature. Upon cooling back to the initial temperature, the diffraction peak positions of the re-solidified sample are consistent with the diffraction pattern of the initial state, which proves that the cell structure of the DNAN/NA cocrystal can be restored to its initial state after thermal cycling.

Similarly, as shown in Fig. 3b and S3b,† the XRD curve of the ADN/urea cocrystal does not exhibit new characteristic diffraction peaks when heated to 65 °C, but the diffraction peaks gradually shift toward decreasing 2θ values as the temperature rises. For example, the diffraction peak of the (0 0 4) crystal plane shifts from $2\theta = 18.371°$ to 18.293°, indicating thermal expansion of the crystal structure within this temperature range. When the heating temperature exceeds 70 °C, the diffraction peaks gradually disappear, indicating that the cocrystal melted at this temperature. When the temperature returns to the initial temperature, comparison with the initial state diffraction pattern reveals that the diffraction peak positions remain essentially unchanged, proving that the sample retains its cocrystal phase after melting–solidification. The above studies show that despite the DNAN/NA and ADN/urea cocrystals undergo lattice expansion and melting during heating, they are still cocrystal phases upon gradual cooling to room temperature. Therefore, using DNAN/NA and ADN/urea cocrystals as melt-cast carriers effectively prevents the occurrence of phase separation crystallization during the melt-casting process of multi-component carriers, thereby impacting on the performance of melt-cast explosives.

3.3 Scanning electron microscope

The DNAN/NA and ADN/urea cocrystals were melted and cooled. After solidification, microstructure changes were observed by SEM, as shown in Fig. 4. The microstructure of the ADN/urea cocrystal remains largely unchanged before and after melting–solidification, exhibiting a long rod shape. Fig. 4c shows the scanning electron microscope image of the DNAN/NA cocrystal sample before melting–solidification, revealing rod-like crystal. Fig. 4d shows a scanning electron microscope image of the DNAN/NA cocrystal after melting–solidification, showing that the morphology remains rod-like, although a small amount of solid phase aggregation appears on the sample surface due to rapid cooling during solidification. Overall, the micromorphology of both cocrystal explosives exhibits minimal change before and after melting–solidification, with the crystal morphology being successfully restored to its initial state.

3.4 Solubility of CL-20 in melt-cast carrier

The solubility of the high energy density material CL-20 in the molten states of DNAN, DNAN/NA, and ADN/urea was accurately determined at 100 °C using high performance liquid chromatography with standard curve method. The results of the solubility calculation are summarized in Table 1. The solubility of CL-20 in the two cocrystal carriers was significantly lower than that of CL-20 in DNAN. Notably, the solubility of CL-20 in the inorganic salt cocrystal carrier ADN/urea (1.046 g) is much lower than that in the traditional organic cocrystal carrier DNAN/NA (3.274 g), this may be attributed to the fact that CL-20 belongs to organic matter and is more likely to be dissolved in organic carriers with similar polarity in the two carriers with large differences in polarity.

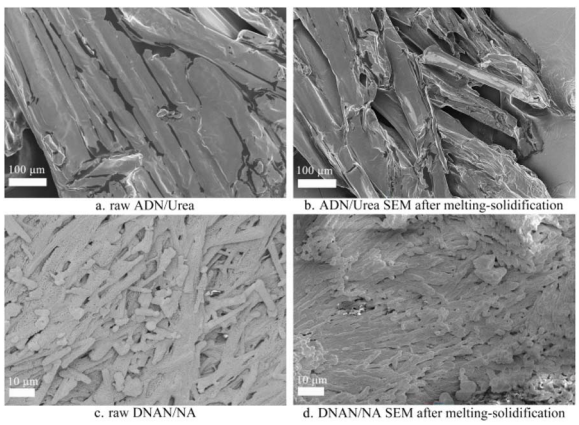

Fig. 4 SEM of ADN/urea and DNAN/NA cocrystals.

Table 1 Solubility of CL-20 in DNAN, DNAN/NA and ADN/urea

Sample	S/(g·100 g^{-1})			$\bar{S}$/(g·100 g^{-1})
DNAN	10.045	10.423	9.378	9.949
DNAN/NA	3.347	3.243	3.233	3.274
ADN/urea	1.108	1.155	0.876	1.046

3.5 The polymorphic transformation of CL-20 in melt-cast carrier

The polymorphic transformation behavior of ε-CL-20 in two different types of cocrystal melt-cast carriers, DNAN/NA and ADN/urea, was studied by X-ray powder diffraction at 100 °C, as shown in Fig. 5 and S4.† For ε-CL-20 in the DNAN/NA, the main diffraction peaks of ε-CL-20 mainly appeared at 12.55°, 13.82°, 16.31°, 21.95°, and 30.32°. These peak positions were consistent with those obtained from the simulated ε-CL-20 CIF file using Mercury software, confirming the absence of any other crystalline forms. Indicating that ε-CL-20 did not undergo polymorphic transformation during the melting and casting process when DNAN/NA served as the carrier. Similarly, the XRD pattern Fig. 5b of ε-CL-20 in the ADN/urea cocrystal carrier showed that the diffraction peaks identical to those of standard ε-CL-20, and there is no characteristic diffraction peak of other crystal forms.

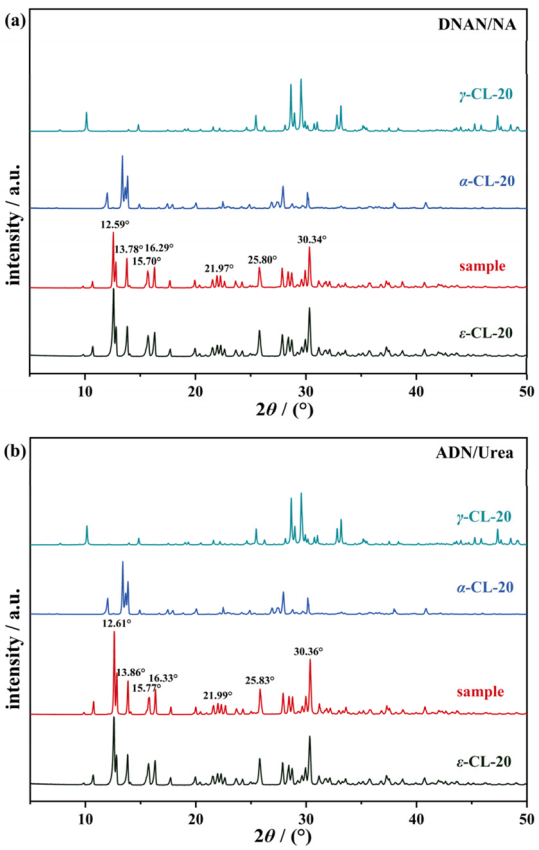

Fig. 5 (a) XRD patterns of ε-CL-20 in DNAN/NA carrier, (b) XRD patterns of ε-CL-20 in ADN/urea carrier.

Therefore, ε-CL-20 maintained its crystal structure during the melting and casting processes when ADN/urea acted as the carrier.

4 Conclusions

In this study, DNAN/NA and ADN/urea cocrystals were prepared by solvent evaporation method, and their feasibility as melt-cast explosive carriers was analyzed. The key findings are summarized as follows:

(1) The thermal stability of DNAN/NA and ADN/urea cocrystals was studied. The results show that the melting point and decomposition temperature of DNAN/NA and ADN/urea cocrystals were 69.3 °C, 71.9 °C and 319.8 °C, 201.9 °C, respectively. Notably, the difference between melting point and decomposition temperature exceeded 100 °C for both cocrystals, satisfying the thermal performance requirements for melt-cast explosive carriers.

(2) The crystal structure changes of two cocrystal carriers at different temperatures, as well as the microstructural changes before and after melt–solidification were analyzed by *in situ* XRD and SEM. The results show that despite the DNAN/NA and ADN/urea cocrystal experiencing lattice expansion and melting phenomena during the temperature rise, the re-solidified samples after undergoing thermal cyclic loading still retain their cocrystalline phase. The phase separation crystallization of the cocrystal carrier during the casting process was avoided, which affected the performance of the explosive.

(3) The solubility of CL-20 within DNAN/NA and ADN/urea cocrystal carriers were studied by HPLC. The results demonstrated that the solubility of CL-20 in the two cocrystal carriers was 3.274 g and 1.046 g, respectively, significantly lower than that of CL-20 in pure DNAN (9.949 g). Furthermore, the polymorphic transformation of ε-CL-20 in the process of melt-casting was analyzed by XRD. The results show that the ε-CL-20 remained stable in both melt-cast cocrystal carriers without undergoing polymorphic transformation.

Data availability

The authors confirm that all data supporting this study are available within the article and its ESI.†

Author contributions

Y. Zhao: conceptualization, methodology and writing original draft. Y. Zhou, J. Song and F. Wang: writing review & editing, methodology and date analysis. X. Zhou and X. Zhang: methodology, XRD and SEM measurements. L. Su, Z. Suo and J. X: supervision, writing review & editing. S. Sun and J. Sun: conceptualization, supervision, funding acquisition, writing review & editing. All authors have read and agreed to the published version of the manuscript.

Conflicts of interest

There are no conflicts to declare.

Acknowledgements

This work was supported by the PhD Project of Southwest University of Science and Technology (no. 22zx7134).

Notes and references

1 C. M. Yu, F. Tian and S. K. Liu, *Equipment Manufacturing Technology*, 2017, vol. 7, pp. 95–96+108.
2 H. X. Wang, X. F. Wang and Y. M. Luo, *Explos. Mater.*, 2021, **50**, 1–9.
3 Z. L. Yang, A. Li, Y. Yu, J. Y. Guo and Q. J. Li, *J. Ordnance Equip. Eng.*, 2022, **43**, 193–200.
4 Q. J. Li, Z. L. Yang, X. Yue, J. Y. Guo and A. Li, *J. Ordnance Equip. Eng.*, 2023, **44**, 125–132.
5 F. Hu, Y. C. Liu, J. M. Yuan, L. J. Wang and Q. A. Huang, *J. Ordnance Equip. Eng.*, 2021, **42**, 1–6.
6 M. I. Eremets, I. A. Trojan and A. G. Gavriliuk, *Static Compression of Energetic Materials*, 2008, pp. 75–97.
7 P. Yin, J. H. Zhang, G. H. Imler, D. A. Parrish and J. M. Shreeve, *Angew. Chem.*, 2017, **129**, 8960–8964.
8 X. Hao, Z. W. Ye and X. L. Zhou, *Chin. J. Explos. Propellants*, 2023, **46**, 16–30.
9 C. Li, Y. Q. Yu and G. J. Zhang, *J. Mater. Sci.*, 2024, **59**, 14172–14184.
10 P. Ravi, D. M. Badgujar, G. M. Gore, S. P. Tewari and A. K. Sikder, *Propellants, Explos., Pyrotech.*, 2011, **36**, 393–403.
11 B. H. Zheng, G. Luo, Y. J. Shu and P. S. Wang, *Chem. Ind. Eng. Prog.*, 2013, **32**, 1341–1346.
12 F. Chen, Y. C. Liu, Y. Wang and Q. H. Zhang, *Chin. J. Energetic Mater.*, 2020, **28**, 1109–1119.
13 T. M. Klaptke, *Nat. Chem.*, 2023, **15**, 1480.
14 M. Anniyappan, K. Vijay Varma, R. S. Amit and J. K. Nair, *J. Energ. Mater.*, 2020, **38**, 111–125.
15 N. Sikder, A. K. Sikder, N. R. Bulakh and B. R. Gandhe, *J. Hazard Mater.*, 2004, **113**, 35–43.
16 Z. Jalový, S. Zeman, M. Sućeska, p. Vávra, K. Dudek and M. Rajić, *J. Energetic Mater.*, 2001, **19**, 219–239.
17 A. I. Kazakov, D. V. Dashko, A. V. Nabatova, A. I. Stepanov and D. B. Lempert, *Combust. Explos. Shock Waves*, 2018, **54**, 147–157.
18 Y. Li, J. M. Yuan, W. Zhao, Y. Qu, X. W. Xing, J. W. Meng and Y. C. Liu, *Russ. J. Gen. Chem.*, 2021, **91**, 445–455.
19 Y. J. Li, D. L. Cao, Y. X. Li, Y. Du and J. L. Jian, *Chin. J. Explos. Propellants*, 2013, **36**, 28–30.
20 L. Chen, Y. J. Shu, R. J. Xu, X. Tao and X. F. Wang, *Chin. J. Energetic Mater.*, 2013, **21**, 108–115.
21 S. Sheng, B. Jin and R. F. Peng, *Chin. J. Energetic Mater.*, 2023, **31**, 970–978.
22 B. B. Li, Y. M. Luo, W. Lei, M. M. Zhang and W. Wang, *Chin. J. Energetic Mater.*, 2021, **29**, 308–314.
23 X. Y. Feng, Q. Xue, J. L. Zhang, K. D. Yang, K. K. Wang, B. Z. Wang and F. Q. Bi, *R. Soc. Chem. Adv.*, 2024, **14**, 36980–36988.
24 L. J. Wang, F. Hu, S. M. Jing, Y. C. Liu, J. W. Zhu, J. X. He and S. H. Zhang, *Chin. J. Explos. Propellants*, 2021, **44**, 658–664.
25 J. W. Zhu, L. J. Wang, Y. C. Liu, J. H. Wang, M. Tian, Y. J. Duan and Q. Z. Bin, *Chin. J. Energetic Mater.*, 2022, **30**, 228–235.
26 X. L. Song, Y. Kou, Y. Wang, Z. P. Cheng and F. S. Li, *J. Energ. Mater.*, 2022, **40**, 119–135.
27 L. Y. Chen, T. You, Y. M. Liao, Q. Tian and X. H. Duan, *Chin. J. Explos. Propellants*, 2023, **46**, 441–448.
28 Z. S. Julio and E. R. T. Tiekink, *CrystEngComm*, 2007, **9**, 833–834.
29 A. Nangia, *J. Chem. Sci.*, 2010, **122**, 295–310.
30 C. Y. Zhang, Y. Xiong, F. B. Jiao, M. M. Wang and H. Z. Li, *Cryst. Growth Des.*, 2019, **19**, 1471–1478.
31 C. A. Gunawardana and C. B. Aakeröy, *Chem. Commun.*, 2018, **54**, 14047–14060.
32 S. H. Sun, H. B. Zhang, J. J. Xu, S. M. Wang, C. H. Zhu, H. F. Wang, R. Q. Ding, Z. H. Yu and J. Sun, *Cryst. Growth Des.*, 2019, **19**, 6826–6830.
33 S. Qiao, Z. W. Yang, H. Z. Li, Y. W. Yu, Y. C. Liu and J. H. Wang, *Chin. J. Energetic Mater.*, 2021, **29**, 1182–1185.
34 S. Qiao, J. H. Wang, Y. H. Yu, Y. C. Liu, Z. W. Yang and H. Z. Li, *CrystEngComm*, 2022, **24**, 2948–2953.
35 M. K. Bellas and A. J. Matzger, *Chem. Sci.*, 2022, **13**, 12100–12106.